STRESS CORROSION CRACKING BEHAVIOUR OF LOW ALLOY STEELS IN HIGH TEMPERATURE WATER: DESCRIPTION AND RESULTS FROM MODELLING

B. Tirbonod

The initiation and growth of a crack by stress and corrosion in the low alloy steels used for the pressure vessels of Boiling Water Reactors may affect the availability and safety of the plant. This paper presents a new model for stress corrosion cracking of the low alloy steels in high temperature water. The model, based on observations, assumes the crack growth mechanism to be based on an anodic dissolution and cleavage. The main results deal with the position of the dissolution cell found at the crack tip, and with the identification of the parameters sensitive to crack growth, among which are the electrolyte composition and the cleavage length. The model is conservative, in qualitative agreement with measurements conducted at PSI, and may be extended to other metal-environment systems.

1 INTRODUCTION

Stress corrosion cracking is the initiation and growth of a crack under the simultaneous synergetic effects of an approximately constant tensile stress and a chemically active environment in a susceptible material.

The phenomenon is observed in metals covered by a passivating oxide film, which protects the metal from further corrosion. It can be briefly explained as follows for the case of a crack growth by anodic dissolution, one of the mechanisms considered in this work. A local rupture of the film by stress generates a potential drop between the local bare surface of the metal and the passivated metal. The current generated gives rise to the dissolution of the bare metal, resulting in crack initiation or growth. The return of the metal to its original state, due to growth of the film by electrochemical reactions, arrests the dissolution till the next film rupture.

The occurrence of stress corrosion cracking requires a critical stress or strain for rupture of the film, which is environment dependent, and a value of the potential at the surface of the metal in the range of values where the film is unstable, to allow the anodic dissolution and repassivation. This phenomenon has the potential to be observed in a broad range of metal-environment systems.

The main characteristics of stress corrosion cracking include the value of the critical stress, which can be smaller than the yield stress, the uncertainty about the identification of the parameters for a given metal-environment system, the sensitivity to slight changes in the values of the parameters (which can remain out of control, and result in crack initiation or growth at any time during the life of the component), and the difficulty of detection for crack lengths smaller than a few millimetres. These facts make stress corrosion cracking potentially dangerous for a structure.

The critical parameters are the local residual and external stresses, the local composition of the metal, and the environment. The mechanisms differ according to the metal-environment system, even if they are similar from a macroscopic point of view.

For nuclear reactor technology, the behaviour of the low alloy steels in high temperature water is of interest because these steels are the base material of the reactor pressure vessel. It is important to know whether stress corrosion cracking can occur in these materials, after eventual cracking of the cladding of the pressure vessel, and to identify the conditions for crack growth, since these issues are relevant to the safety of the plant (failure of the vessel resulting in a major accident), and to the availability and life-time extension (the vessel is the only component which cannot be replaced). Experiments have shown a large scattering of results: five orders of magnitude for the crack growth rate, and related model uncertainties [1].

Although relevant parameters for the phenomenon can be identified, there is no assurance that all the critical parameters have been recognized.

The present paper summarizes the theoretical work conducted in the framework of the PSI/HSK project "SpRK von Stählen für Reaktor-Komponenten in Heisswasser" [1,2]. The goal of this work is to identify the critical parameters of stress corrosion cracking behaviour of low alloy steels in high temperature water, by considering the phenomena in the region of the crack tip using a phenomenological model.

The paper includes descriptions of the stress corrosion cracking models cited in the literature for the cases of low alloy steels in high temperature water, the assumption of a crack growth mechanism, and the new models developed at PSI for calculating crack growth. Finally, the results are presented and discussed.

2 DESCRIPTIONS OF STRESS CORROSION CRACKING IN LOW ALLOY STEELS AND MODELS FROM THE LITERATURE

The water in the pressure vessel of a Boiling Water Reactor is characterised by the presence of dissolved species, such as oxygen, hydrogen peroxide, hydrogen (due to radiolysis), and impurities [3]. Tests conducted with pre-cracked specimens in an electrolyte simulating this water (in terms of composition, temperature and pressure) have shown that the critical species for stress corrosion cracking in low alloy steels in high temperature water are the oxidising species (dissolved oxygen, hydrogen peroxide), which control the value of the electrochemical corrosion potential, sulphate ions, and sulphur compounds gen-

erated by the dissolution of manganese sulphide inclusions of the metal in the region of the crack tip [1].

Two descriptions of stress corrosion cracking have been proposed for these steels in the literature (Fig. 1, [4,5]). Both assume for the crack growth mechanism an anodic dissolution initiated by the rupture of the oxide film.

The first description (Fig. 1b, [4]) assumes that the dissolved oxygen is reduced in a differential aeration cell in the region of the crack mouth. This results in an electrolyte free of oxygen at the crack tip, due to the fact that for oxygen the reduction rate overcomes the diffusion rate along the crack. This results in an electrochemical potential gradient developing along the crack. The consequence is an enrichment of ions developing in the region of the crack tip, by migration in the potential gradient, and by diffusion. The dissolution cell is situated in the region of the crack tip. The anodic reaction of the dissolution cell is the oxidation of Fe, and the cathodic reaction is the reduction of H^+ resulting from the dissociation of H_2O.

The second (Fig. 1a, [5]) assumes that the dissolution cell occupies the whole crack, with as anodic reaction the oxidation of Fe at the crack tip, and as cathodic reaction the reduction of oxygen on the crack surface exterior to the crack itself.

A quantitative model calculating the crack growth rate has been proposed for each description.

The PLEDGE model [6], proposed for the first description, is of semi-empirical nature, directly derived from experiments. This model calculates the crack growth rate as a function of the stress intensity factor, and of other measurable parameters, for direct application to practical cases.

The Coupled Environment Fracture Model [6], proposed for the second description, is of a phenomenological nature. The model uses the transport and potential equations, together with charge conservation, allowing the calculation of the water chemistry along the crack for the composition of the electrolyte assumed at the crack mouth. The model calculates the crack growth rate as a function of the stress intensity factor, and of the composition of the water at the crack mouth.

These models exhibit uncertainties, or questionable assumptions [2]. Both use a relationship between the stress intensity factor and the strain rate at the crack tip for which no support by finite element calculation exists, and there is only one mechanism for the crack growth. The semi-empirical character of the PLEDGE model provides only empirical information on the mechanisms by which the parameters act upon the crack growth. The Coupled Environment Fracture Model exhibits uncertainties for the assumption about the position of the cathode, and of its area, and does not consider that the potential and the concentrations constitute implicit functions for the solution of the equations. For these reasons, these models have not been used in the present work.

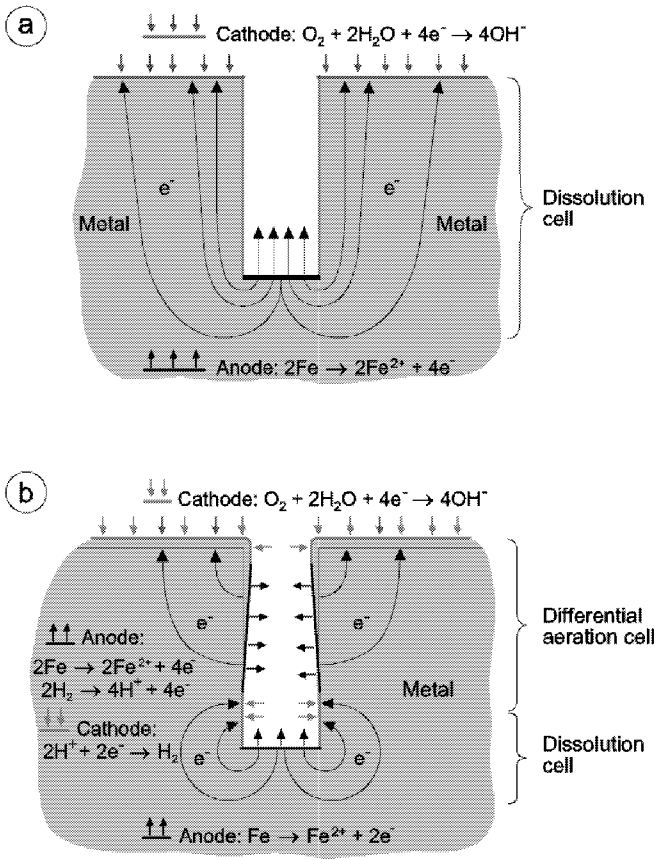

Fig. 1: Description of stress corrosion cracking: (a) by the Coupled Environment Fracture Model and (b) by the PLEDGE model.

3 MODELS DEVELOPED AT PSI

3.1 Assumption of a Crack Growth Mechanism

A literature review for metals [2,7] has shown that there are no common crack-growth mechanisms for stress corrosion cracking at the microscopic level, and that modelling should be based on observations of the particular metal/environment system. For the case of low alloy steels in high temperature water, the ongoing oxidation during the test destroys the original micrographic structure, impeding, for these steels, the direct identification of the mechanism from analysis of the crack surface [1]. Therefore, for these steels, an assumption must be made for the crack growth mechanism.

The low potential and the presence of an oxide layer of magnetite on the crack surface (characteristic of a low content of dissolved oxygen in the water at 288°C), the large sensitivity of the crack growth to the content of sulphur compounds in the water (characteristic of an active repassivation), the necessity of a relevant plastic yielding, and the existence of a critical strain for the initiation of the stress corrosion cracking, all support the following hypothesis for the crack growth mechanism [1,2]:

The oxide film covering the metal is locally ruptured at the crack tip due to the large strains present in this

region. This generates a local bare surface of the metal and the anodic dissolution. Simultaneously, the oxide film nucleates and grows, which decreases the dissolution current; the dissolution is arrested when the film has reached a critical thickness. A cleavage is then generated in the region of the dissolution cavity, and coalesces with it (Fig. 2). This cleavage represents all the other phenomena having potential to contribute to the crack growth.

3.2 Structure of the Model

The description of stress corrosion cracking which will be chosen for modelling will be that assuming a differential aeration cell at the crack mouth, and the dissolution cell in the region of the crack tip (Fig. 2). There is experimental support for this representation.

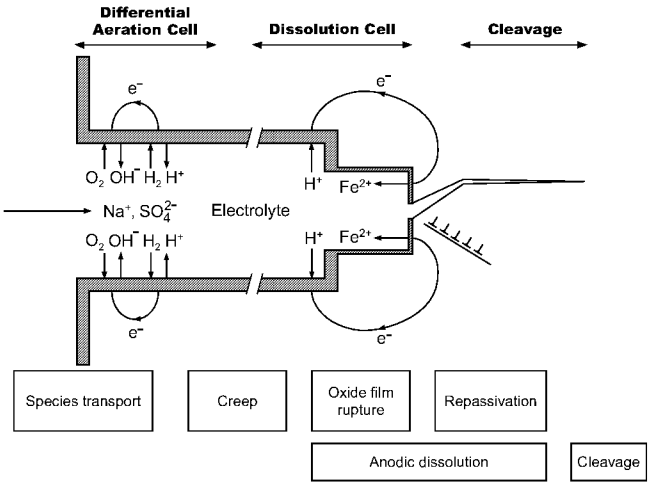

Fig. 2: Phenomena assumed to be involved in stress corrosion cracking of low-alloy steels in high temperature water.

The above-mentioned crack growth mechanism can be described in partial models, each representing a particular phenomenon (Fig. 2 and Fig. 5).

The first (partial) model calculates the number of film ruptures, and the strain at the crack tip, for a given value of the stress intensity factor. These parameters govern the crack growth (there is no crack growth if there is no film rupture). The second calculates the crack growth length by dissolution for a given film rupture event by taking into account the effect of the nucleation and growth of the oxide film on the dissolution current density, in close connection with the composition of the electrolyte. The cleavage length and the composition of the electrolyte at the crack tip will be considered as parameters [2].

The equations for the number of film ruptures, together with those for the crack growth length by dissolution, determine the equations for the crack growth for the mechanism of stress corrosion cracking assumed here, and for an assumed value of the cleavage length (Table 1).

Table 1: Equations for the crack growth.

Number of film ruptures

Time interval $\tau_{f,i}$ between two film ruptures at times t_i and t_{i+1}:

$$\tau_{f,i} = t_{i+1} - t_i$$

Recursive calculation of t_i:

$$\varepsilon_{ct}(t_{i+1}) - \varepsilon_{ct}(t_i) = \varepsilon_f$$

Number of film ruptures N(Δt) within time Δt:

N(Δt)= max (i)

Abbreviations:

ε_{ct} = crack tip strain, ε_f = strain to film rupture

Crack growth by dissolution

Dissolution propagation length a_d per film rupture event:

$$a_d = \frac{M_{Fe}}{nF\rho_{Fe}} \int_0^{\tau_d} i_d \, dt$$

Dissolution current density i_d:

$$i_d = \begin{cases} i_{d,0} & 0 < t < t_0 \\ i_{d,0}(t/t_0)^{-p} & t_0 < t < \tau_p \\ 0 & t > \tau_p \end{cases}$$

Dissolution time τ_d:

$$\tau_d = \begin{cases} \tau_f & 0 < t < \tau_p \\ \tau_p & t > \tau_p \end{cases}$$

Abbreviations:

M_{Fe}, ρ_{Fe} = atomic mass and density of iron

n = stoichiometric number of electrons

F = Faraday number

t = time

$i_{d,0}$ = maximum value of the dissolution current density

t_0 = film nucleation time, p = exponent

τ_p = repassivation time

Crack growth

$$a = a_0 + \sum_i^{N(\Delta t)} (a_{d,i} + a_c)$$

Abbreviations:

a = crack growth length, a_0 = initial crack length,

a_c = cleavage length

$a_{d,i}$ = dissolution propagation length at film rupture number i

3.3 Model for the Number of Film Ruptures

The number of film ruptures within a given time interval will depend on the time interval between two successive film ruptures τ_f. The equations for calculating τ_f as a function of time are given in Table 1; the parameters are the strain at the crack tip $\varepsilon_{ct}(t)$ and the critical strain for the film rupture ε_f .

The strain at the crack tip is directly derived from the Crack Tip Opening Displacement [2]. This has been calculated as a function of time for a pre-cracked C(T) specimen (thickness 25 mm) made from low alloy steel at 288°C, and for a loading which includes a dynamic phase (to bring the load to a specific value), and a static phase at this load [9]. The calculations used the model of Chaboche for the constitutive law of the metal, and employ the finite element method for the solution. The phase considered for the model will be the static phase, for which the strain exhibits a low temperature or logarithmic behaviour for the 30 years considered. The calculations have been made with the assumption of small-scale yielding to allow transfer of the results to the components. This assumption is fulfilled for the specimen loaded at a stress intensity factor of 30 MPa·m$^{1/2}$, and for a crack-growth length not exceeding about 5 mm [2,9]. The effect of the crack-growth length on the strain has not been considered for these calculations.

3.4 Model for the Dissolution Propagation Length

3.4.1 Model for the Film Nucleation and Growth

The dissolution propagation length per film rupture event (dissolution propagation length), a_d, will be calculated from the dissolution current density i_d using Faraday's law (Table 1). The dissolution current density must include the initiation and growth of the oxide film. This is done using an empirical equation derived from experiments for the dissolution current [6]. The kinetics of the film include a nucleation phase, characterised by the film nucleation time t_0, for which the dissolution current density i_d remains at its maximum value $i_{d,0}$, a growth phase (or repassivation), for which i_d decreases with a rate given by an exponent, denoted by p, and the arrest of the dissolution (full repassivation), for which i_d will be assumed to be zero. The parameters t_0 and p are environment dependent. In the model, the value of t_0 will be assumed to be constant, and that of p to depend only on the sulphate concentration.

3.4.2 Calculation of $i_{d,0}$

A new model had to be developed to calculate $i_{d,0}$. The reason is that the models from the literature for calculating the dissolution current are not reliable since they do not consider charge conservation [2].

Charge conservation is related to the areas of the anode and cathode, implying the need to consider three dimensions for the dissolution cell for proper representation. At present, the only way to do this is to assume the electrolyte to be homogeneous in the dissolution cell; i.e., species transport will not be considered in this cell [2].

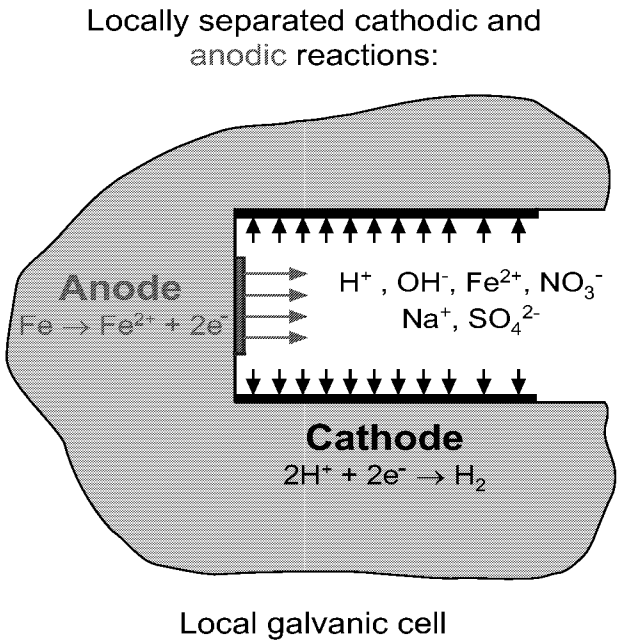

Fig. 3: Outline of the dissolution cell.

This assumption, which provides a maximum case for the dissolution propagation length, is conservative [2]. Note that the dissolution current density is proportional to the cathode to anode area ratio A_c/A_a for a given value of the cathodic current density (Table 2). This parameter explicitly appears in the charge concentration.

The three-dimensional dissolution cell (Fig. 3) is assumed to lie in the region of the crack tip, with the anode over the tip itself, and two squared cathodes, each situated on a particular side of the crack. The height of the cell is the Crack Tip Opening Displacement.

The metal embedding the crack is assumed to be pure iron, which simulates the low alloy steel for the anodic dissolution. The electrolyte includes water and the ions H^+, OH^-, Fe^{2+}, NO_3^-, Na^+, SO_4^{2-} resulting from the dissociation of H_2O, $Fe(NO_3)_2$ and of Na_2SO_4, respectively. The anodic reaction is the oxidation of Fe, and the cathodic reaction the reduction of H^+ (Fig. 3). The concentrations of the Fe^{2+} and H^+ ions determine the voltage source for the dissolution. The sulphate ions act upon the repassivation kinetics, while the nitrate ions remain neutral [4,8]. The sulphate ions represent those provided by the electrolyte outside the crack by transport, as well as the sulphur compounds resulting from the dissolution of the manganese sulphides.

The electrolyte is assumed to be dilute, of constant composition, chemically neutral, electroneutral, homogeneous, at constant temperature, and at rest. The Fe^{2+} and H^+ ions produced and consumed, respectively, at the electrodes will not be considered. The equations are given in Table 2. The model uses the charge conservation, Ohm's law, and the Butler-Volmer law.

Table 2: Equations for the dissolution cell.

Charge conservation:

$$I_a + I_c = 0$$

$$I_a = i_a A_a$$

$$I_c = i_c A_c$$

Ohm's law:

$$\phi_c - \phi_a = R_e I_a$$

Butler-Volmer law:

$$I = i_0 A\left(\exp\left(\frac{\phi-\phi_0}{\beta_a}\right) - \exp\left(-\frac{\phi-\phi_0}{\beta_c}\right)\right)$$

Nernst law:

$$\phi_0 = \phi^0 + \frac{RT}{nF}\ln C$$

$$i_{d,0} = \frac{I_a}{A_a}$$

Abbreviations:

R = perfect gas constant

T = temperature

C = concentration of Fe^{2+} or H^+

I = current[1]

i = current density[1], i_0 = exchange current density[1,2]

A = electrode area[1]

ϕ = potential[1], ϕ_0 = equilibrium potential[1,2]

ϕ^0 = standard potential[1] at temperature T

R_e = electrolyte resistance

β_a = Tafel coefficient of the partial anodic reaction[1,3]

β_c = Tafel coefficient of the partial cathodic reaction[1,3]

Ohm's law connects the current to the potential through the resistance of the electrolyte. The Butler-Volmer law [8] connects, for a given electrode, the current to the potential through the polarisation resistance of the electrode. For this latter law, the relevant variable is the exchange current density, which expresses the charge transfer rate at equilibrium [8]. The equilibrium potential of a given electrode is given by the Nernst law, assumed to depend only on the concentration of the species reacting at the electrode. The resistance of the electrolyte is numerically calculated by assuming straight current lines in the cell for a given conductivity of the electrolyte [2].

The anodic and cathodic potentials, as well as the dissolution current, are numerically determined for given values of the parameters (Fig. 4).

[1] Subscript "a" (anodic) or "c" (cathodic) is omitted

[2] $i_{a,0}$, $i_{c,0}$, $\Phi_{a,0}$, $\Phi_{c,0}$

[3] $\beta_{a,a}$, $\beta_{a,c}$;$\beta_{c,a}$, $\beta_{c,c}$

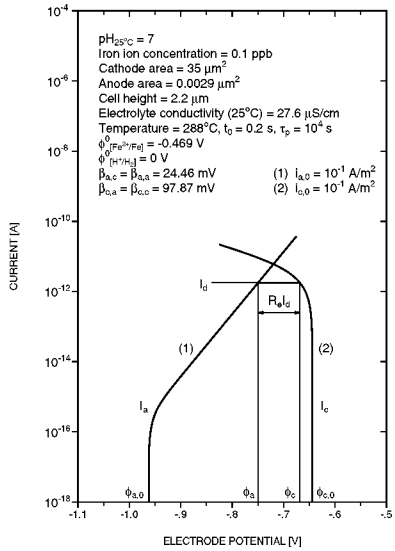

Fig. 4: Determination of the anodic and cathodic potentials and the dissolution current I_d.

It appears that the equilibrium potentials determine, from their difference, the voltage source for the dissolution, which will depend thereby on the concentrations of the reacting species. The values of the anodic potential are found in the instability region of the oxide film, made from magnetite for the potential (-0.75 V, [2]), in agreement with one feature of the stress corrosion cracking mechanism.

3.7 Crack Growth in Connection with Strain and Corrosion

The equations of the crack growth (Table 1) show that the process is governed solely by the strain at the crack tip; the corrosion acts only on the amplitude of the dissolution propagation length a_d.

The amplitude of the crack growth results from two contributions: the strain at the crack tip, for a given value of the strain to film rupture ε_f, by the number of film ruptures, the corrosion, by the values of a_d, and the cleavage length a_c (Tables 1 and 2). The value of a_d depends on the strain at the crack tip, on ε_f, and on the value of the time interval between two film ruptures. For this reason, there will generally be no correlation between the crack growth and the strain at the crack tip.

With this description, there are no synergetic effects between crack growth and corrosion, effects which can result in a delayed and unstable growth of the crack [2].

Figure 5 schematically shows, as functions of time, the load applied to the pre-cracked specimen, the resulting strain at the crack tip, the times of occurrence of the film ruptures (for a constant value of the strain to film rupture), the dissolution current, and the crack growth length induced by the anodic dissolution and cleavage. One notes that the kinetics of the crack growth depend strongly on the time interval between two film ruptures τ_f, in relation to the film nucleation time t_0 and to the repassivation time τ_p.

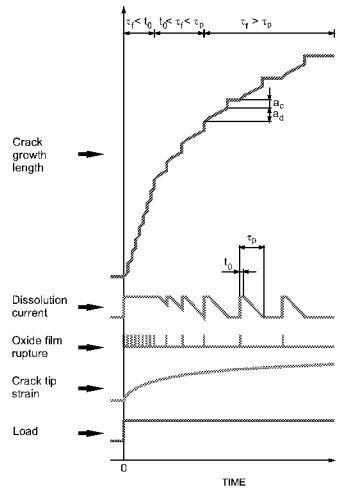

Fig. 5: Load versus time and resulting strain at the crack tip, oxide film rupture events, dissolution current, and crack growth length.

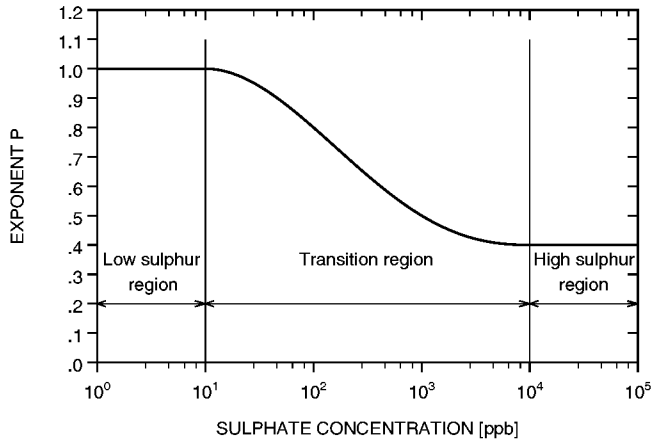

Fig. 6: Value of p versus sulphate concentration.

4 RESULTS

4.1 Values of the Parameters

The main parameters of the model for electrochemistry are the concentrations of iron and sulphate ions, and the exchange current densities [2]. The values of these parameters will be chosen to provide extreme cases for the crack growth, while still remaining realistic [2]. The concentrations will be 0.1 ppb for Fe^{2+}, and in the range from 1 to 10^5 ppb for the sulphate ions. The value of t_0 is 0.2s [2]. The value of p varies between 1 and 0.4 for sulphate concentrations in the range 10 to 10^4 ppb, and remains constant outside this interval at the latter value (Fig. 6, [2]). The repassivation time is chosen to be conservative (10^4 s). The electrical conductivity of the electrolyte increases linearly with the concentrations [8]. For the crack growth, in relation to the film ruptures, the main parameter is the strain-to-film rupture ε_f, which will take the minimum value from the literature (of the order of 10^{-3}). This corresponds to the emergence of the order of 10^2 dislocations by creep, this number determining also the anode height (0.029 µm). With an anode width of 0.1 µm (dislocation mean length in steel), the anode area is 0.0029 μm^2. The cathode length or area is unknown, and the value should be determined for given values of the parameters (see later).

A requirement for consistent application of the model is that the cathode length is in excess of the cell height. For a stress intensity factor of 30 $MPa \cdot m^{1/2}$, the cell height is 2.2 µm [9], which will be the lower bound for the cathode length, with corresponding values of about 4.8 μm^2 for the cathode area, and of about 1670 for the cathode to anode area ratio. The consequence will be a significant reduction for the values of the anodic and cathodic exchange current densities $i_{a,0}$ and $i_{c,0}$, respectively, which can be considered here. These values will be at maximum 10^{-1} A/m^2 [2], which is relatively small compared with the maximum value of 10^4 A/m^2 from the literature (range of possible values: 10^{-8} to 10^4 A/m^2, [8]).

The cleavage length will take the values of 0, 1, and 10 µm, this last value being taken from micrography [1].

A threshold value of 10^{-3} µm will be assumed for the dissolution propagation length for consideration of crack growth related to a given film rupture (crack growth event). This comes from the fact that this length cannot be smaller than an inter-atomic distance, and must overcome a threshold value for activating a second crack growth mechanism such as cleavage.

4.2 Dissolution Cell

Figure 7 shows that, for a given anode area, a_d increases as a function of the cathode length to reach a maximum, and then decreases at higher values. The increasing phase is due to the effect of the cathode to anode area ratio, and the decreasing phase to the ohmic resistance in the electrolyte due to the increasing dimensions of the cell. The position of the maximum depends on the values of the parameters [2], as shown in Fig. 7 for the case of the cathodic exchange current density $i_{c,0}$ for the maximum value of the anodic exchange current density $i_{a,0}$. This Figure also shows the dependence of a_d on $i_{c,0}$, which decreases by a factor of roughly 10 for a decrease of $i_{c,0}$ by a factor 10^5. When the values of the exchange current densities are equal, this factor is much larger (about 10^4, [2]).

The value of the cathode length providing the maximum of a_d will be the estimate of the cathode length of the dissolution cell for the given values of the parameters. This length does not exceed about 300 µm, the larger values being found at low exchange current densities [2]. This shows that the dissolution cell is situated in the region of the crack tip for a long crack, a major result of the model.

Figure 8 shows the dependence of a_d on the conductivity of the electrolyte at the crack tip for two different electrolytes. The first is predominant for sulphate ions, while the second includes sulphate ions (at given concentrations) as well as iron and nitrate ions.

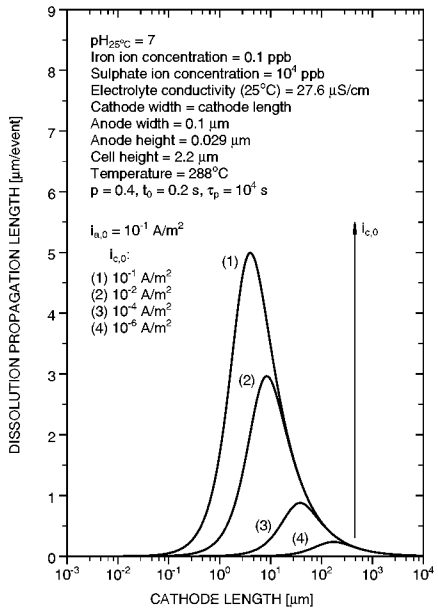

Fig. 7: Dissolution propagation length versus cathode length.

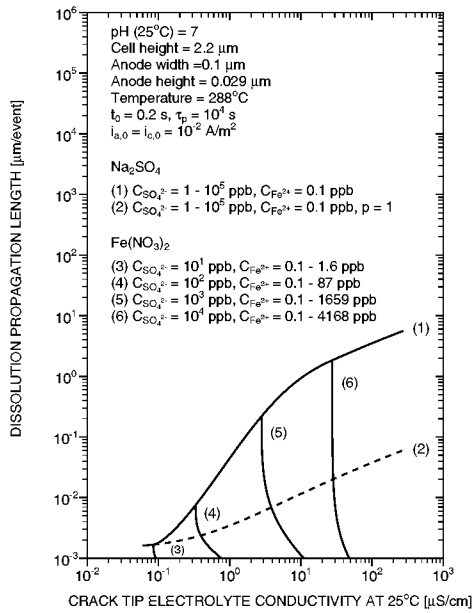

Fig. 8: Dissolution propagation length versus conductivity for two electrolytes of different compositions.

For the first electrolyte, a_d increases as a function of the conductivity. The rate increase for sulphate concentrations in the range from 10 to 10^4 ppb, for which the kinetics of the oxide film growth, or the value of the exponent p, varies; this is in agreement with experiments. The effect of the repassivation on the value of a_d for a given conductivity can be estimated by comparing the value with that obtained by assuming for p the value 0.4 (obtained for the sulphate concentration of 10 ppb) for all the sulphate concentrations. For this value, the repassivation rate is the largest; i.e., the value of a_d is the smallest. One sees that the effect of the repassivation is to increase a_d by a factor up to about 10^2 at a given conductivity.

For the second electrolyte, a_d decreases as a function of conductivity for increasing concentrations of the Fe^{2+} and NO_3^- ions. This is due to the fact that increasing Fe^{2+} concentration increases the value of the anodic equilibrium potential $\Phi_{a,0}$, the equilibrium cathodic potential $\Phi_{c,0}$, given by the H^+ concentration, remaining constant. This results in a decreasing value of the voltage source $\Phi_{c,0} - \Phi_{a,0}$ available for the dissolution and, consequently, the same for a_d.

This latter result means that the crack growth can be slowed down at increasing conductivity, which has been observed (though for simultaneous increase of the pH [4]), or arrested, if the value of a_d does not exceed the threshold value.

These results show that the decisive parameter for anodic dissolution is the composition of the electrolyte, not the conductivity. The composition determines the voltage source, the conductivity, and the repassivation. The effect of the voltage source overcomes those of the conductivity and repassivation if its value becomes small. If this occurs, the crack growth will be slowed down, or arrested, whatever the value of the conductivity. This result is a consequence of the assumption of homogeneity of the electrolyte, and can be used for testing the assumption.

4.3 Crack Growth

Figure 9 shows that the crack growth length monotonically increases as a function of time for any value of the sulphate concentration, and for any cleavage length. The effect of repassivation can be seen by comparing the form of the curve obtained for the sulphate concentrations of 10^5 ppb at zero value of the cleavage length with the forms of the other curves.

For any value of the sulphate concentration, and for any cleavage length, the crack growth does not exceed a few millimetres [2], which fulfils the assumption of small-scale yielding for the relatively small value of the exchange current densities i_0 considered here. One notes that the same value of the crack growth can result from a large value of the sulphate concentration with a small value of the cleavage length, and vice versa. This means that a small value of the conductivity does not imply a small value of the crack growth. One also notes that the crack growth can be delayed.

The delay can amount, for very low values of i_0, to about $1.6 \cdot 10^5$ s (44 hours). This is due to the contribution of time to the value of a_d when the contributions of the other parameters are too small to allow a_d to overcome the threshold value of 10^{-3} µm for initiating the crack growth at a film rupture [2].

4.4 Comparison with Experiments

Measurements [1] have shown no crack growth for the case of K_I = 30 MPa·m^{½}, even with an aggressive electrolyte outside the crack (for the given oxygen content), and for a conductivity of 0.5 µS/cm (corresponding to 165 ppb of sulphate ions). This result confirms the conservative character of the model for stress corrosion cracking if extreme cases are assumed.

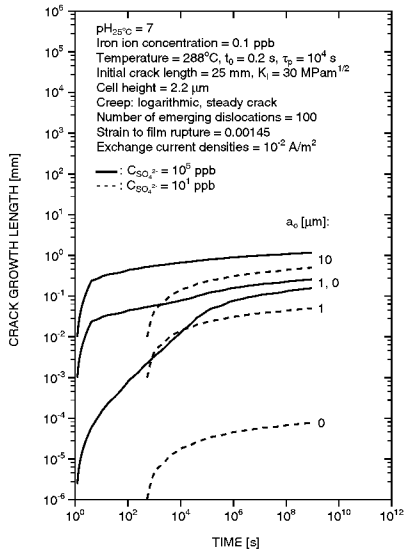

Fig. 9: Calculated crack growth length versus time.

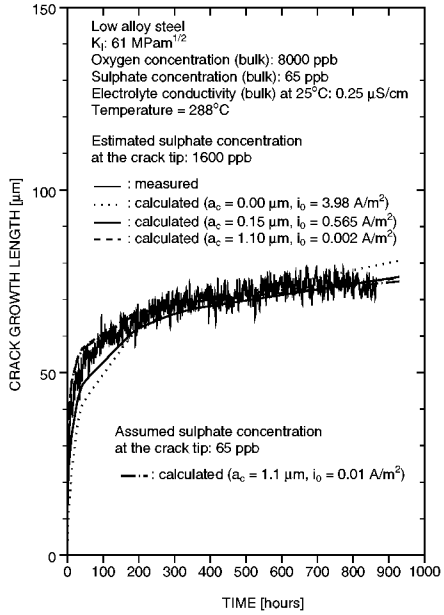

Fig. 10: Qualitative comparison of the crack growth length calculated from the model with that measured [1,2].

The first measurement considered has been obtained for a specimen made from a low alloy steel in water at 288°C containing 8000 ppb of oxygen and 65 ppb of sulphate ions (Fig. 10, [1]). These two latter values lead us to expect a value of roughly 1600 ppb for the sulphate concentration at the crack tip [4]; the value of K_I was 60 MPa·m^{½}. The crack growth length has been measured by the reversed direct current potential drop method.

The calculated values of the crack growth length are in qualitative agreement with those measured (Fig. 10, [2]). Several sets of values for the sulphate concentration, exchange current densities, and cleavage length, could be considered, the agreement being improved when the cleavage contributes to the crack growth.

The other measurements considered will be those obtained by Rising Displacement Tests, conducted up to a maximum value of 61 MPa·m^{½} for K_I, with an electrolyte containing oxygen (8000 ppb) and sulphate ions (65 ppb, [1]). These measurements show that the crack growth rate depends only on the Crack Opening Displacement Rate; i.e., on the crack-tip strain rate. Therefore, they can be interpreted with the present model.

Figure 11 shows the measured points together with those calculated by assuming for the cell height the constant value of about 9.1 µm (k_I= 60 MPa·m$^{1/2}$ [9]), and for a sulphate concentration at the crack tip of 1600 ppb. For several values of the strain to film rupture, cleavage length and exchange current densities, there is good agreement. All give for the strain to film rupture a value of the order of 10^{-3}, and a non-zero value for the cleavage length [2].

These results qualitatively support the model, and confirm that an additional mechanism to the anodic dissolution should be considered for the crack growth.

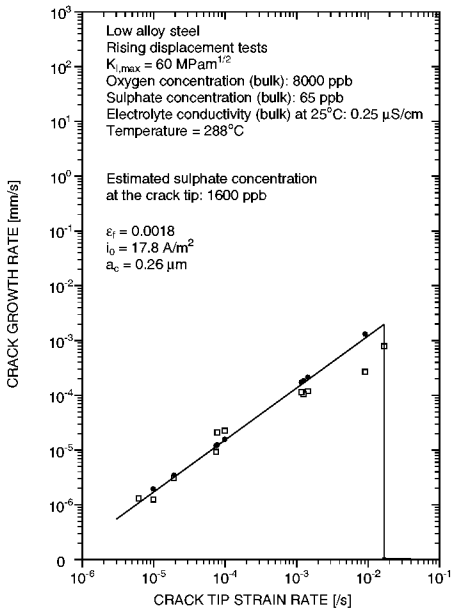

Fig. 11: Crack growth rate versus crack tip strain rate obtained by Rising Displacement Tests (▫, [1]), and by the present model (•, [2]).

5 DISCUSSION AND CONCLUSIONS

The present model calculates the crack growth as a function of time for the case of small-scale yielding, the main parameter being the composition of the electrolyte at the crack tip. The assumption of homogeneity of the electrolyte provides a maximum case for the crack growth.

In spite of its relative simplicity, and of its assumptions and limitations, the following new, and non-trivial, results could be obtained using the model.

5.1 Main Results of the Model

(a) The critical parameters for crack growth include the values of the exchange current densities, the composition of the electrolyte at the crack tip, the strain to film rupture for a given strain at the crack tip as a function of time [2], and the cleavage length. Although these results could be derived from a qualitative analysis of the model, the model has provided a quantitative evaluation of their impact on the crack growth, which can be complex, and partly explains the scattering of the experimental results.

(b) The major result of the model is that the dissolution cell is situated in the region of the crack tip. Its extension along the crack does not exceed a few hundred micrometers, depending on the sulphate concentration and the exchange current densities.

This result is consistent with the description of stress corrosion cracking assumed here, which is based on experiments. It does not support the assumption of a pre-defined length for the dissolution cell (the crack length), as in models from the literature for dissolution [2] or stress corrosion cracking [5]. The cathode length must be determined by the model itself, and depends on the parameters of the model.

The model can be applied for all cracks of length in excess of a few hundred micrometers (which excludes application to corrosion pits). For these cracks, the dissolution cell will be electrically disconnected from the differential aeration cell present in the region of the crack mouth. This justifies the assumption of the reduction of H^+ in the cathodic reaction for the case of low alloy steels in high temperature water. However, the dissolution cell remains chemically coupled to the electrolyte external to the crack by the migration induced by the differential aeration cell, and by diffusion.

(c) Another important result of the model is the effect of the composition of the electrolyte, which can lead to drastic crack growth, according to the species present. Two different effects have been found.

The first deals with the species which delay repassivation at increasing concentrations (sulphate ions here), which increases the dissolution rate at a given time. It appears that the effect of the repassivation can drastically overcome that of the conductivity for the dissolution propagation length by up to a factor 10^2. The second deals with the species determining the values of the anodic and cathodic equilibrium potentials; i.e., of the voltage source. This effect is closely connected to the concentrations of the species at the electrode, where they electrochemically react. If the value of the voltage source, which governs the dissolution, thereby tends to zero, the dissolution will be slowed down or arrested, whatever the values of the other concentrations determining the conductivity or the kinetics of the repassivation. If dissolution is arrested, crack growth will also be arrested.

(d) Qualitative evaluation of the model with experiments confirms that a second mechanism for crack growth, in addition to the anodic dissolution, should be considered. This is a new result compared with other models for stress corrosion cracking of steels in high temperature water, which consider only the dissolution [5,6].

(e) Finally, the model is very conservative (no crack growth could be observed in the limits of the detection threshold $K_I = 30\ MPa{\cdot}m^{1/2}$ considered for the calculations for aggressive conditions [1]). This means that the value of the crack growth calculated with the present model can be considered as an upper bound, taking extreme values for the parameters. This can be of interest for safety purposes for which only knowledge of an upper bound value is sufficient for a given set of conditions.

5.2 Application of the Model and Extension to other Metal-Environment Systems

The application of the model requires determination of the values of the exchange current densities, which must be separately measured for the metal-environment system under consideration, since they cannot be predicted [8]. The determination of these current densities allows comparisons of calculated crack growth against measurement for evaluating the model. It allows also the determination of the values of the crack-tip parameters ε_f and a_c. These parameters, which cannot at present be directly measured for the case of low alloy steels in high temperature water, are critical for the amplitude of the crack growth. Two very different concentrations of sulphate ions in a deoxygenated electrolyte outside the crack should be considered for these experiments.

The structure in terms of partial models, each representing a particular mechanism, allows direct application of the model to any metal-environment system for which the present crack growth mechanism can be assumed, given the appropriate values of the parameters and the constitutive law for the material.

ACKNOWLEDGMENTS

This work has been financially supported by the Swiss Federal Office for Energy (BFE) and by the Swiss Federal Nuclear Safety Inspectorate (HSK).

REFERENCES

[1] J. Heldt, U. Ineichen, H.P. Seifert, B. Tirbonod, U. Tschanz, "*Stress Corrosion Cracking of Low Alloy Steels in High Temperature Water*", PSI Report, to be published.

[2] B. Tirbonod, "*Modelling of the Stress Corrosion Cracking Behaviour of Low Alloy Steels in High Temperature Water*", PSI Report, Nr. 00-08 (2000).

[3] J. Hickling, U. Reitzner, "*Water Chemistry Aspects of Corrosion Cracking taking BWR Plants as an Example*", VGB Kraftwerkstechnik, **72**, 341-349 (1992).

[4] P.L. Andresen, L.M. Young, "*Characterization of the Roles of Electrochemistry, Convection and Crack Chemistry in Stress Corrosion Cracking*", Proc. Seventh Int. Symposium on Environmental Degradation of Materials in Nuclear Power Systems, NACE, 579-596 (1995).

[5] D.D. Macdonald, M. Urquidi-Macdonald, "*Coupled Environment Model for Stress Corrosion Cracking in Sensitive Type 304 Stainless Steel in LWR Environment*", Corr Sci., **32**, 51-81 (1991).

[6] F.P. Ford, "*Slip Dissolution Model*", in Corrosion sous Contraintes, Phénomélogie et Mécanismes, D. Desjardins and R. Oltra (eds), 307-344 (1992).

[7] T. Magnin, "*Advances in Corrosion Deformation Interactions*", Trans Tec Publications (1995).

[8] D. Landolt, "*Corrosion et Chimie des Surfaces des Métaux*", Presses Polytechniques et Universitaires Romandes, Sections 4 and 5 (1993).

[9] D.Z. Sun, M. Sester, R. Mohrmann, R. Westerheide, H. Riedel, and H. Yuan, H.P. Seifert, and H. Heldt, "*Berechnung des Spannungs-und Deformationszustandes in der Umgebung eines Risses unter korrosiven Bedingungen*", Report V 158/98 of the Fraunhofer Institut für Werkstoffmechanik, Freiburg (D) and Paul Scherrer Institut, Villigen (CH), 1998.